PNAS RESEARCH ARTICLE | BIOPHYSICS AND COMPUTATIONAL BIOLOGY

Structural rewiring of IL-7R dimerization by an oncogenic transmembrane mutation can be reversed by rational design

Qian Wang[a,b,1], Min Chen[a,1], Asma Lasram[c,1], Saana Vihuri[d], Angela Z. Chou[a], Weixin Bian[a,e], Zhiming Dai[a,e], Outi Haapanen[d], Giray Enkavi[d], Christoph Pollmann[c], Ilpo Vattulainen[d], Tiantian Cai[f,2], Jacob Piehler[c,2], and James J. Chou[a,b,e,2]

Affiliations are included on p. 11.

Edited by Alessandro Senes, University of Wisconsin, Madison, WI; received January 16, 2026; accepted March 31, 2026 by Editorial Board Member Anthony A. Kossiakoff

Mutations within the transmembrane domains (TMDs) of single-pass transmembrane receptors often cause aberrant, ligand-independent receptor signaling associated with diverse malignancies, but their mechanism of action remains largely unknown. These TMD mutations are generally not targetable as they are buried in the membrane. Here, we determined the mechanism of a gain-of-function (GOF) TMD mutation of interleukin-7 receptor (IL-7R) associated with T cell acute lymphoblastic leukemia and addressed the possibility of directly targeting the TMD mutation by using rationally designed transmembrane helices to restore order to uncontrolled signaling. We find that the GOF mutation of IL-7R severely shifts the TMD homodimerization interface, causing the receptor to homodimerize in a geometry that activates downstream signaling independent of ligand. Designed transmembrane helices that interfere with the new interface, delivered with mRNA technology, selectively block ligand-independent but not ligand-dependent signaling. Our study provides a conceptual framework for understanding and repairing disease-causing TMD mutations of single-pass cytokine receptors.

IL-7R | oncogenic transmembrane mutation | disease mechanism | therapeutic design

Significance

Mutations in transmembrane domains (TMDs) of cytokine and immune receptors often cause aberrant, ligand-independent signaling linked to diverse malignancies, but the mechanisms are largely unknown. This paper reveals an oncogenic mutation within the IL-7 receptor TMD completely alters the receptor's dimerization mode, causing activation without a ligand and T cell acute lymphoblastic leukemias. The study also demonstrates the effective use of rationally designed transmembrane (TM) peptides to repair this aberrant signaling. Our work suggests that understanding the structural basis of how a TM mutation modulates receptor conformation makes it possible to use designed TM peptides to specifically suppress these issues. We believe similar approaches could help understand and repair disease-causing TM mutations for many other cytokine receptors.

Many single-pass cytokine and growth factor receptors harbor mutations in the transmembrane domain (TMD) that cause ligand-independent receptor activation and diseases. These mutations are often not cysteine substitutions that could force receptor oligomerization via disulfide formation. Hence, their effect on signaling should be attributed to changes in conformation and/or oligomerization. Delineating the disease mechanism of these mutations necessitates a deeper understanding of receptor mechanism beyond ligand-induced conformational changes, which may provide previously unrecognized opportunities for therapeutic interventions.

The first report of a single-pass transmembrane (TM) receptor harboring a major oncogenic TMD mutation was on the neu/p185 receptor (rat equivalent of the human erb-b2 receptor tyrosine kinase HER2), of which the residue V664 in the TMD is mutated to Glu (1). Analogous oncogenic TMD mutation V659E in human HER2 has also been identified to be an oncogenic driver of lung adenocarcinomas and is associated with poor prognosis in non–small lung carcinoma patients (2). Unexpectedly, these charge-introducing mutations within the membrane, which are generally perceived as disruptive, can cause constitutive activation of neu and HER2, respectively (1, 2). Although the precise mechanism of the TMD mutations remains elusive, the findings suggested that the receptor TMD is not merely a membrane anchor but plays an active role in receptor dimerization and activation (2). Selective inhibition of TMD mutation-induced oncogenic signaling remains an unsolved problem.

In addition to receptor tyrosine kinases, oncogenic noncysteine mutations in the TMD have been identified in several class I cytokine receptors. A S505N mutation in the thrombopoietin receptor (TpoR) results in constitutive TpoR activation and essential thrombocythemia (3, 4). This mutation is believed to promote a mode of TpoR TMD dimerization that activates downstream signaling independent of thrombopoietin (5). TMD mutations leading to ligand-independent signaling have also been reported for members of the common γ-chain (γc; also known as IL-2Rγ) family of interleukin receptors. For example, a recurrent hotspot mutation I242N in the IL-4R TMD was found in patients with primary mediastinal large B cell lymphoma and can lead to JAK/STAT activation that does not depend on IL-4 (6).

More importantly, the TMD of IL-7R has emerged as a hotspot of oncogenic mutations involving both cysteine and cysteine-less mutations and insertions accounting for about

The authors declare no competing interest.

This article is a PNAS Direct Submission. A.S. is a guest editor invited by the Editorial Board.

Copyright © 2026 the Author(s). Published by PNAS. This article is distributed under Creative Commons Attribution-NonCommercial-NoDerivatives License 4.0 (CC BY-NC-ND).

[1]Q.W., M.C., and A.L. contributed equally to this work.

[2]To whom correspondence may be addressed. Email: tiantiancai@zju.edu.cn, piehler@uos.de, or james_chou@mail.sioc.ac.cn.

This article contains supporting information online at https://www.pnas.org/lookup/suppl/doi:10.1073/pnas.2601748123/-/DCSupplemental.

Published April 28, 2026.

Downloaded from https://www.pnas.org by CAS SHANGHAI TECH UNIVERSITY on June 11, 2026 from IP address 119.78.253.17.

10% of IL-7R mutations associated with T cell acute lymphoblastic leukemias (ALL) (7–11). IL-7R is also a member of the γc family of cytokine receptors that plays important roles in the development, proliferation, and homeostasis of T and B cells (12–14). Under normal circumstances, IL-7R needs to specifically heterodimerize with γc upon IL-7 binding to allow activation of downstream STAT5 phosphorylation via the Janus family tyrosine kinases JAK1 and JAK3 (14–17). A previous structural study revealed that the TMDs of IL-7R and γc can specifically interact in the membrane with a knob-into-hole mode of association and this interaction synergizes with ligand-induced heterodimerization of IL-7R and γc in activating downstream signaling (18). A transmembrane mutation of IL-7R (V253G) found in some patients with ALL, however, is able to activate IL-7R without the ligand (9, 10), possibly by directly promoting homodimerization of the intracellular JAK1 and trans-activation (19, 20).

In this study, we sought to uncover the structural and mechanistic basis by which the transmembrane mutation V253G causes ligand-independent IL-7R signaling, and explore the possibilities of interfering with such oncogenic signaling via rationally designed transmembrane helices. To this end, we combined the use of the bicelle NMR technology, single-molecule FRET, bacterial two-hybrid assays, functional mutagenesis, as well as molecular dynamics (MD) simulation to investigate the coupling between the TMD structure and intracellular JAK1 activation exploited by the disease mutation to activate the receptor without ligand. We find that the V253G mutation can completely alter the intrinsic dimerizing property of the TMD, resulting in a new type of TMD homodimerization that synergizes with auto-cross-activation of JAK1s. By means of a transmembrane peptide antagonist, we achieved selective inhibition of oncogenic homomeric signaling of IL-7R V253G while not interfering with the ligand-dependent receptor activation via γc.

Results

The V253G Mutation Caused TMD Homotypic Association Interface to Rotate by ~170°. As mentioned above, the human IL-7R TMD mutation induces constitutive STAT5 phosphorylation in BaF3 cells (9), and V253 is also a hotspot for insertion mutations (*SI Appendix*, Fig. S1*A*). WT or V253G IL-7R was expressed in BaF3 cells with or without γc, and STAT5 and JAK1 phosphorylation were measured as an indicator of receptor activation. Cell surface expression of WT and mutant IL-7Rs was very similar except for modestly higher level of the mutant when coexpressed with γc (*SI Appendix*, Fig. S1 *B*–*E*). Coexpression of γc and WT IL-7R showed ~5 times stronger p-STAT5 and ~3 times stronger p-JAK1 upon IL-7 treatment (*SI Appendix*, Fig. S1 *F* and *G*), whereas V253G exhibited strong p-STAT5 and p-JAK1 signals in the absence of IL-7 regardless of coexpression with the γc or not (*SI Appendix*, Fig. S1 *F* and *G*). Based on the above results and those previously reported by others (9, 10), we conclude that the disease mutation V253G of IL-7R can activate downstream STAT5 phosphorylation independently of the cognate ligand IL-7 and such ligand-independent p-STAT5 signal appeared to be comparable to the IL-7-induced p-STAT5 of the WT IL-7R in our expressed receptor system.

To investigate the structural effect of the V253G mutation by NMR, we reconstituted the IL-7R TMD with the point-mutation V253G (designated IL-7Rtm-V253G) in POPC-DH_6PC bicelles (*SI Appendix*, Fig. S2) that mimic a lipid bilayer (21–24). To avoid biased dimerization due to disulfide bond formation, we substituted Cys261 by His, which is found at this position in mouse and rat IL-7R variants (*SI Appendix*, Fig. S3). After the assignment of backbone amide and sidechain methyl chemical shifts (*SI Appendix*, Fig. S4), we examined dimerization contacts by measuring NMR nuclear Overhauser effects (NOE). In this experiment, uniformly ^{15}N-labeled and perdeuterated IL-7Rtm-V253G was mixed with ^{13}C-labeled IL-7Rtm-V253G for exclusive detection of NOEs between amide protons of the (^{15}N, ^{2}H)-labeled chain with nonlabile protons of the ^{13}C-labeled chain (22). The results show that the backbone amides of F250, V257, and A260 exhibited strong interchain NOEs (Fig. 1*A*). In comparison, the backbone amides of the WT IL-7Rtm (IL-7Rtm-WT) showing strong interchain NOEs are that of L255 and L259 (Fig. 1*B*). The change in interchain NOE pattern indicates that the V253G mutation resulted in about 170° rotation of the dominant dimerization interface from the L255 side to the G253 side (Fig. 1*C*). Subsequent full-scale analysis of intra- and interchain NOEs determined the high-resolution structure of the IL-7Rtm-V253G homodimer (Fig. 1*D* and *SI Appendix*, Table S1).

The IL-7Rtm-V253G dimer structure is characterized by a right-handed helical packing mode with a packing angle of ~30°. In the middle of the TMD, the S249-XXX-G253 sequence forms the most intimate interhelical contact. The C-terminal ends of the two TMDs (residue K265) in the dimer are approximately 15 Å apart. The dimeric complex appears to be largely mediated by the small-XXX-small motif that is known to dimerize TM helix in many other single-pass membrane proteins (25–30). The small-XXX-small motif, however, is not the only point of close helical packing as S249 also makes contact with the opposing helix in the dimer interface (Fig. 1*E*). Overall, the structure shows that replacing V253 with Gly has reshaped the face of the TMD involving residues 245, 249, 253, and 257 and turned it into a strongly dimerizing interface. According to our NOE data in Fig. 1*A*, this new face can dimerize stronger than the one involving residues 247, 251, 255, and 259 as the V253G mutation has shifted the dominant interchain NOEs from the L255 side to the V257 side.

Atomistic Simulations Identify Altered Stability and Structural Organization of TMD Dimers. To investigate how the V253G mutation alters IL-7R TMD homodimerization, we performed MD simulations starting from three models: 1) the NMR structure of the V253G IL-7R TMD that dimerizes at residue 253 (designated G253-interface mutant; Fig. 2*A*); 2) the WT IL-7R TMD dimerizing at residue 253, generated with back-mutation of the V253G NMR structure while preserving the dimer interface (designated V253-interface WT; Fig. 2*B*); and 3) a model of the WT TMD dimerizing at residue 255 predicted with Boltz-2, guided by NMR constraints of the WT in Fig. 1*B* (designated L255-interface WT; Fig. 2*C*). All dimers were embedded in POPC lipid bilayers with explicit solvent and ions for atomistic MD simulations.

To compare the intrinsic stability of the dimer interfaces, we performed thermal stability simulations, with the temperature gradually ramped from 310 to 350 K over 200 ns (*SI Appendix*, Table S2). Using the observed dissociation events from these simulations, we inferred dissociation temperatures as a measure of relative interface stability (Fig. 2*D*). G253-interface mutant was the most stable, with only one replicate dissociating across all simulations. V253-interface WT was substantially less stable, with all replicates dissociating by ~335 K. L255-interface WT exhibited intermediate stability, with several replicates remaining associated at 350 K. Overall, these quantified stability profiles suggest that the V253G mutant is substantially more stable than WT variants.

To explore the conformational landscape and potential interconversion between interfaces, we performed extended MD

Downloaded from https://www.pnas.org by CAS SHANGHAI TECH UNIVERSITY on June 11, 2026 from IP address 119.78.253.17.

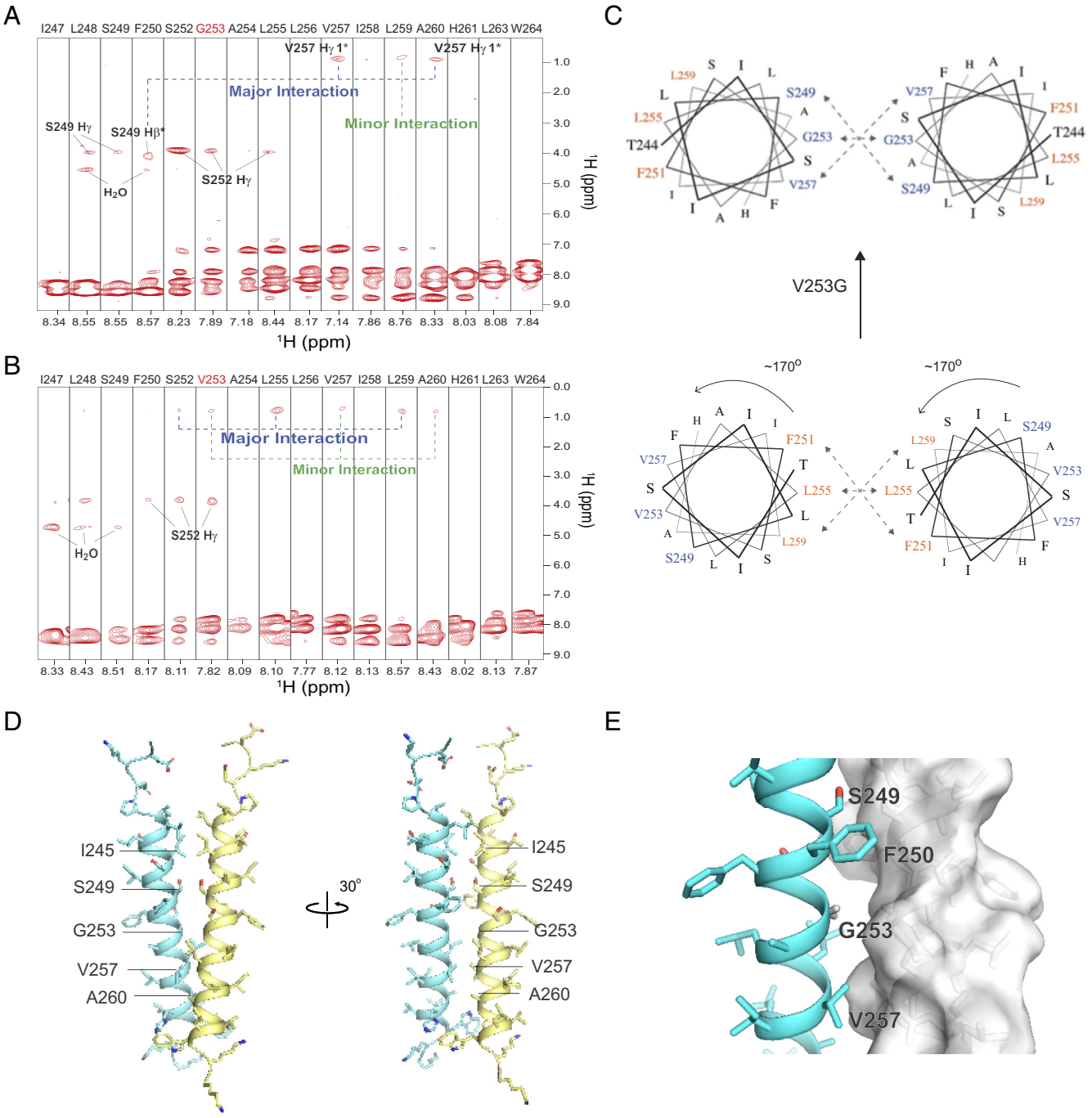


Fig. 1. Major reorganization of the IL-7R TMD dimerization interface caused by the V253G gain-of-function mutation. (*A*) Strips from 3D ^{15}N-edited NOESY–TROSY spectra of (^{15}N, ^{2}H)-labeled IL-7Rtm-V253G randomly mixed with ^{13}C-labeled IL-7Rtm-V253G showing interchain NOEs between the amide protons of (^{15}N, ^{2}H)-labeled chain and nonlabile protons of the ^{13}C-labeled chain. The spectra were recorded at 306 K at ^{1}H frequency of 900 MHz. (*B*) Same type of NMR experiment as in (*A*) recorded with IL-7Rtm-WT at an 800 MHz spectrometer. (*C*) Helical wheel representations of the homodimeric interactions of IL-7Rtm-V253G (*Top*) and IL-7Rtm-WT (*Bottom*), showing that the V253G mutation resulted in ~170° rotation of the helical packing interface. (*D*) Cartoon representation of the IL-7Rtm-V253G dimer structure. (*E*) Surface representation showing the dimer packing interface.

simulations at 310 K for 1 to 2 μs per replicate, with 10 independent repeats per system (*SI Appendix*, Table S2). Clustering analysis of intermolecular distances, reduced to two dimensions via principal component analysis (PCA), identified two compact, well-separated clusters along with dissociated states (*SI Appendix*, Fig. S5*A*). The low within-cluster RMSD compared to the higher between-cluster RMSD confirms that each cluster represents a distinct, well-defined conformational state (*SI Appendix*, Fig. S5*B*). The first cluster, which we call the Mutant-like cluster, corresponds to the G253 mutant interface. The second cluster, which we call the WT-like cluster, corresponds to the L255 WT interface. Analysis of cluster populations showed very limited interconversion between interfaces (Fig. 2*E*). The G253-interface mutant simulations remained almost entirely as the G253 interface, with dissociation below 5%. The V253-interface WT and L255-interface WT simulations exhibited ~10% and ~13% dissociation, respectively. Both systems largely preserved their initial interface; only V253-interface WT showed a minor transition toward the L255 interface (~2%). The observation that the data resolve into just two clusters, each corresponding to an initial interface, with little

Downloaded from https://www.pnas.org by CAS SHANGHAI TECH UNIVERSITY on June 11, 2026 from IP address 119.78.253.17.

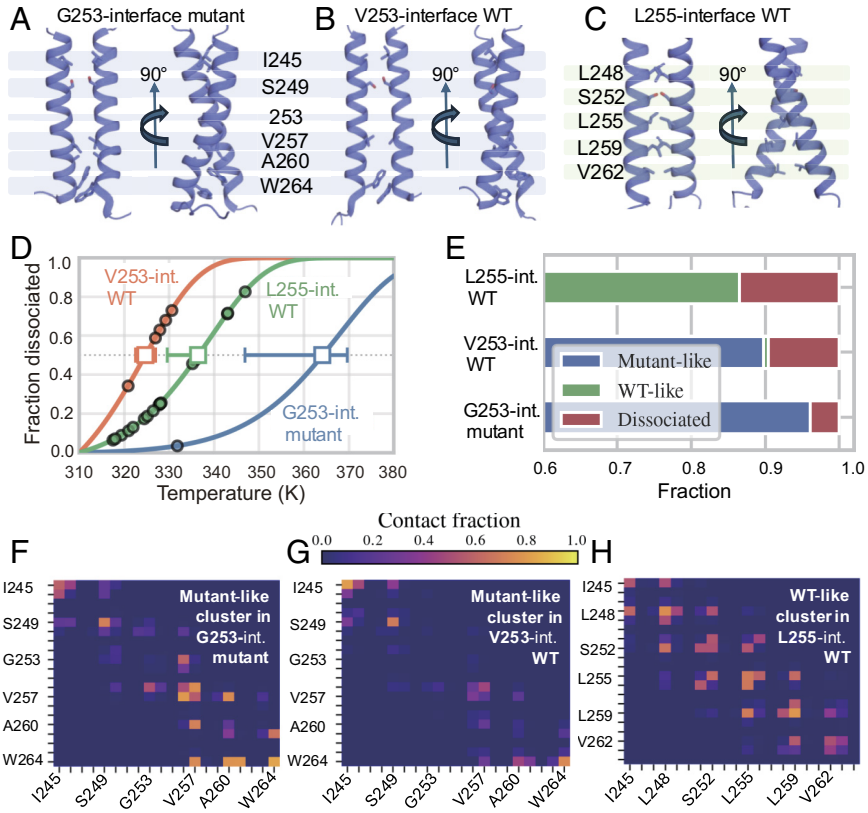


Fig. 2. MD simulations uncover V253G-induced stabilization of IL-7R homodimers. (*A–C*) Cartoon representations of the G253-interface mutant and two WT systems (V253-interface WT and L255-interface WT). The backbone is shown in cartoon and the main interfacial residues are highlighted in stick and labeled. (*D*) Thermostability of dimers from temperature-scan simulations. Survival curves were estimated assuming first-order kinetics with a temperature-dependent Arrhenius rate constant (*Materials and Methods*). The dissociation temperatures (corresponding to 50% survival) are indicated by hollow squares, and error bars represent 95% CI. Data points (circles) show observed dissociation temperatures and are projected onto the survival curves. Even though no corresponding data points are shown, dimers that did not dissociate during the temperature scan (4/5 mutant NMR-based models, 4/21 WT modeled) still contribute to the survival curves and thereby inform the overall stability trends. (*E*) Fraction of replicates in each conformational cluster (interface type) or dissociated state, determined from clustering analysis of equilibrium MD simulations. (*F–H*) Contact frequency maps for Mutant-like and WT-like clusters captured in the G253-interface mutant, V253-interface WT, and L255-interface WT systems. The color bar shown in panel G applies to all maps.

interconversion between them, indicates that these two interfaces dominate the conformational landscape and are separated by an energetic barrier.

Contact analysis of the clustered data reveals the molecular basis for these distinct geometries (Fig. 2 *F–H*). The Mutant-like cluster in G253-interface mutant and V253-interface WT systems are stabilized by additional interactions at I245, S249, I248, L256, V257, and W264 (Figs. 1 *A* and *B* and 2 *F* and *G*). While the signature contact patterns of the Mutant-like interface are captured in both WT and mutant, the WT exhibits fewer contacting residues, likely because of the steric hindrance due to the V253 side chain (compare Fig. 2 *F* and *G*). Notably, W264 sidechains on the intracellular (C-terminal) side of the TMD form aromatic stacking interactions that further stabilize this interface—a feature not captured in the NOE spectra (Fig. 1*B*) and absent in the L255 interface (Fig. 2*H*). In contrast, the WT-like cluster interface exhibits a distinct contact pattern involving I245, I248, S252, L255, L259, and V262, with prominent off-diagonal contacts, suggesting that this interface may be more malleable than the Mutant-like interface.

Analysis of interhelical distance distributions in clustered data reveals distinct geometries for each interface (*SI Appendix*, Fig. S5 *C–E*). The Mutant-like cluster, in both G253-interface mutant and V253-interface WT systems, exhibits extracellular (N-terminal) and intracellular (C-terminal) distances centered around (8 Å, 10 Å), reflecting a relatively parallel helix arrangement. In contrast, the WT-like cluster shows a broader distribution, with the most probable conformation near (10 Å, 17 Å), consistent with a more prominent cross-like helix geometry. Because the intracellular separation determines the relative positioning of the JAKs, these results suggest that the mutation influences not only dimer stability but also its conformation in a manner that could support constitutive activation. Collectively, these MD simulations corroborate that the IL-7R TMD comprises two potential homodimerization interfaces on opposite sides, and that the V253G mutation induces a switch from the L255 to the G253 interface.

TMD Homodimerization at V253G Is Required for Ligand-Independent IL-7R Signaling. We next implemented two independent biochemical experiments for validating the dimerization interface of the V253G mutant TMD. One experiment is based on a bacterial adenylate cyclase two-hybrid (BACTH) assay (Fig. 3*A*) (31). Briefly, two complementary domains (T18 and T25) of adenylate cyclase (AC) were fused, separately, to the TMDs under investigation. The TMD fusion proteins were expressed in an AC deficient (CyaA) strain that yielded white bacteria colonies by default. Stable association of two TMDs reconstitutes AC activity, resulting in blue colonies. Another experiment, named TOXGREEN (Fig. 3*B*), is based on the expression of the super-folded Green Fluorescent Protein (sfGFP) reporter gene, which is driven by the dimerization of the bacterial transcription factor ToXR (32). Specifically, ToXR and MBP (maltose binding protein) are fused to the N- and C- termini of the TMD, respectively, and the fusion protein

Downloaded from https://www.pnas.org by CAS SHANGHAI TECH UNIVERSITY on June 11, 2026 from IP address 119.78.253.17.

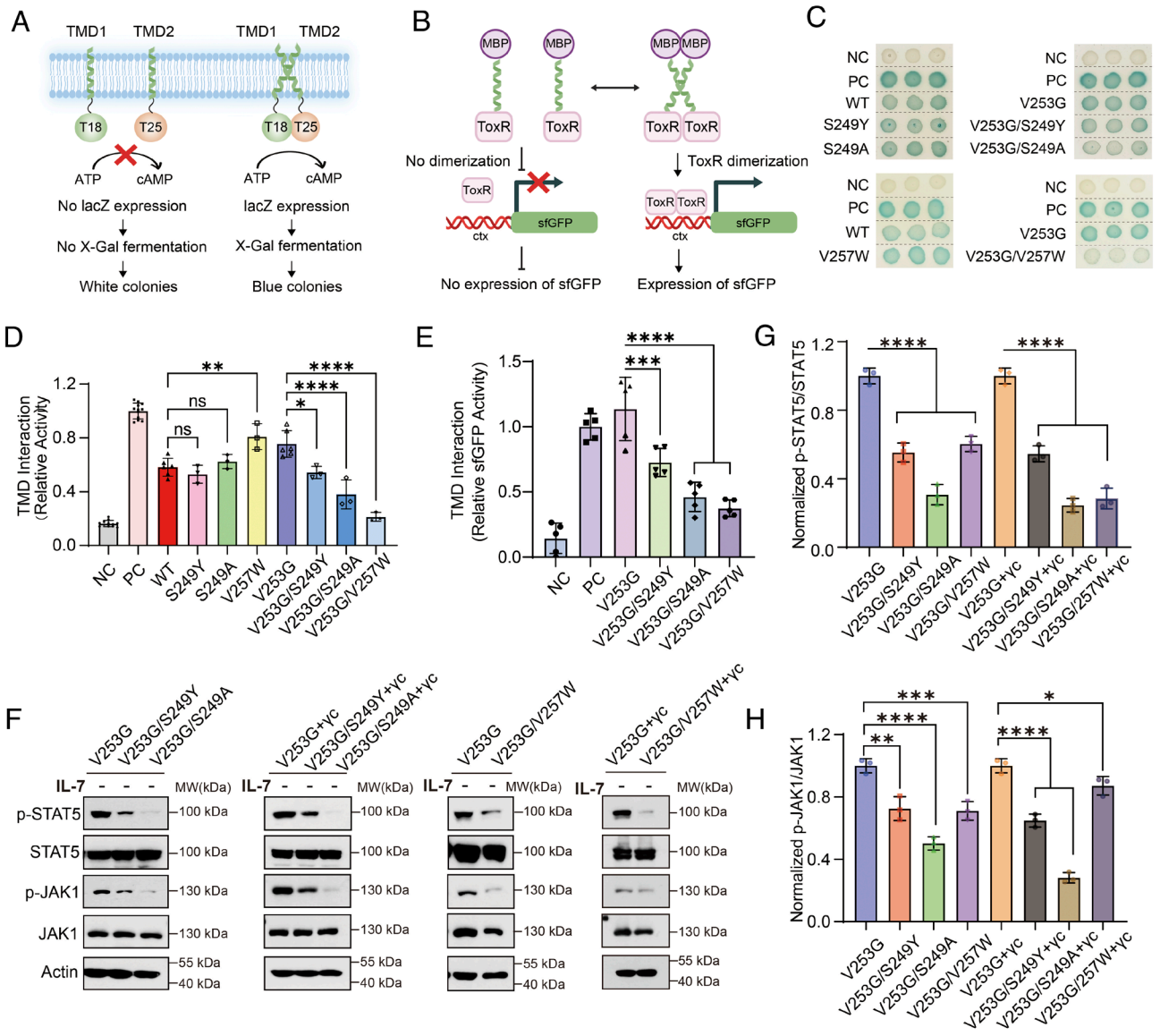


Fig. 3. Requirement of TMD dimerization at the V253G interface by ligand-independent IL-7R signaling. (*A* and *B*) Schematic illustrations of BACTH and TOXGREEN analyses, respectively, used for examining homotypic interactions of IL-7R TMD variants. For the BACTH assay, IbaG/IbaG homodimerization was used as the positive control. For the TOXGREEN assay, glycophorin A (GpA), a classical TM dimer, was used as a positive control, while GpA-G83I, a monomeric mutant, served as the negative control. (*C*) BACTH analysis of TMD interactions for IL-7R TMD variants. Blue colonies indicate interaction between the TMDs in the bacterial inner membrane, while white colonies indicate no such interaction. (*D*) Quantification of BACTH colony colors normalized relative to the IbaG/IbaG positive control. The data are shown as means ± SEMs calculated from technical replicates (typically three) from three independent experiments. Statistical significance by One-way ANOVA. ns, not significant; *$P \le 0.05$; **$P \le 0.01$; ***$P \le 0.001$; ****$P \le 0.0001$. (*E*) TOXGREEN analysis of TMD interactions for IL-7R TMD variants. Quantification of sfGFP activity is normalized relative to the GpA positive control. The data are shown as means ± SEMs calculated from technical replicates (typically five to six) from three independent experiments. Statistical significance by One-way ANOVA. ns, not significant; *$P \le 0.05$; **$P \le 0.01$; ***$P \le 0.001$; ****$P \le 0.0001$. (*F*) Phosphorylation of STAT5 (p-STAT5) and JAK1 (p-JAK1) in BaF3 cells expressing WT or mutant IL-7R or coexpressing with γc. The p-STAT5 and p-JAK1 signals were detected by immunoblotting and compared with total STAT5 and JAK1, respectively. (*G* and *H*) Quantification of p-STAT5 and p-JAK1 signals in (*F*) as p-STAT5/STAT5 and p-JAK1/JAK1 intensity ratios, normalized to the V253G or V253G/γc. The data are shown as means ± SEMs calculated from three independent experiments. Statistical significance by One-way ANOVA. ns, not significant; *$P \le 0.05$; **$P \le 0.01$; ***$P \le 0.001$; ****$P \le 0.0001$.

(ToXR-TMD-MBP) is expressed in the inner membrane of *Escherichia coli* with the MBP domain placed in the periplasm and the ToXR domain in the cytoplasm. Upon TMD dimerization, ToXR binds to the *ctx* promoter and activates the expression of sfGFP.

The results from both assays show that mutating S249 to Tyr on top of the base mutation V253G partially disrupted dimerization by 25 to 35% (Fig. 3 *C–E*). Interestingly, replacing S249 with the smaller Ala, which was considered less disruptive, exhibited more disruptive power and reduced dimerization by 50 to 65% (Fig. 3 *C–E*), suggesting that TMD dimerization is much more complicated than van der Waals (VDW) surface complementarity. Mutating V257 to Trp almost abolished TMD dimerization (Fig. 3 *C–E*), consistent with the dimer structure. These mutagenesis results indicate that the dimer interface of IL-7Rtm-V253G involving S249, G253, and V257 revealed by the NMR structure mediates the homotypic association of IL-7Rtm-V253G in cell membrane.

To determine whether the V253G dimer interface is relevant to ligand-independent IL-7R signaling, we evaluated the effect of the above dimer-breaking mutations on signaling. Full-length WT IL-7R, IL-7R-V253G, IL-7R-V253G/S249Y, IL-7R-V253G/S249A, and IL-7R-V253G/V257W with or without γc were expressed in BaF3 cells. Flow cytometry analysis showed that the membrane

Downloaded from https://www.pnas.org by CAS SHANGHAI TECH UNIVERSITY on June 11, 2026 from IP address 119.78.253.17.

expression levels of these IL-7R variants were nearly the same (*SI Appendix*, Fig. S6). Immunoblotting results show that the V253G mutation generated very significant ligand-independent p-STAT5 and p-JAK1 signals (Fig. 3 *F–H*). The S249Y mutation on top of V253G caused about 50% and 30% reduction in p-STAT5 and p-JAK1, respectively. The S249A mutation reduced p-STAT5 and p-JAK1 signals more than S249Y (Fig. 3 *F–H*), consistent with the TMD dimerization assays (Fig. 3 *C–E*). The V257W mutation on top of V253G also reduced the levels of p-STAT5 and p-JAK1 (Fig. 3 *F–H*). Overall, the results show clear correlation between disruption of V253G TMD dimerization and reduced levels of p-STAT5 and p-JAK1 signals, indicating that IL-7R TMD dimerization at the G253 interface is responsible for the observed ligand-independent JAK1 and STAT5 phosphorylation.

The above results have been independently validated by the STAT5 luciferase reporter assay. In this assay, a BaF3 cell line stably expressing a STAT5-responsive luciferase reporter was used to monitor the STAT5 signaling. Consistent with the immunoblotting data, all three double-point mutants showed significantly reduced luciferase activity (*SI Appendix*, Fig. S7).

The V253G Mutation Causes Ligand-Independent Dimerization of IL-7R in Live Cells. To investigate the relevance of V253G-induced IL-7R TMD dimerization in the physiological context, we quantified receptor diffusion and interaction in the plasma membrane of live cells by single-molecule imaging techniques. IL-7R fused to an N-terminal ALFA tag (ALFA-IL-7R) was constructed, enabling highly selective cell surface labeling using anti-ALFA tag nanobodies (ALFAnb) conjugated with photostable fluorophores (Fig. 4*A*). Activity analysis by phosphoflow cytometry confirmed substantially increased p-STAT5 phosphorylation activity of ALFA-IL-7R V253G compared to WT (*SI Appendix*, Fig. S8*A*). For single-molecule imaging,

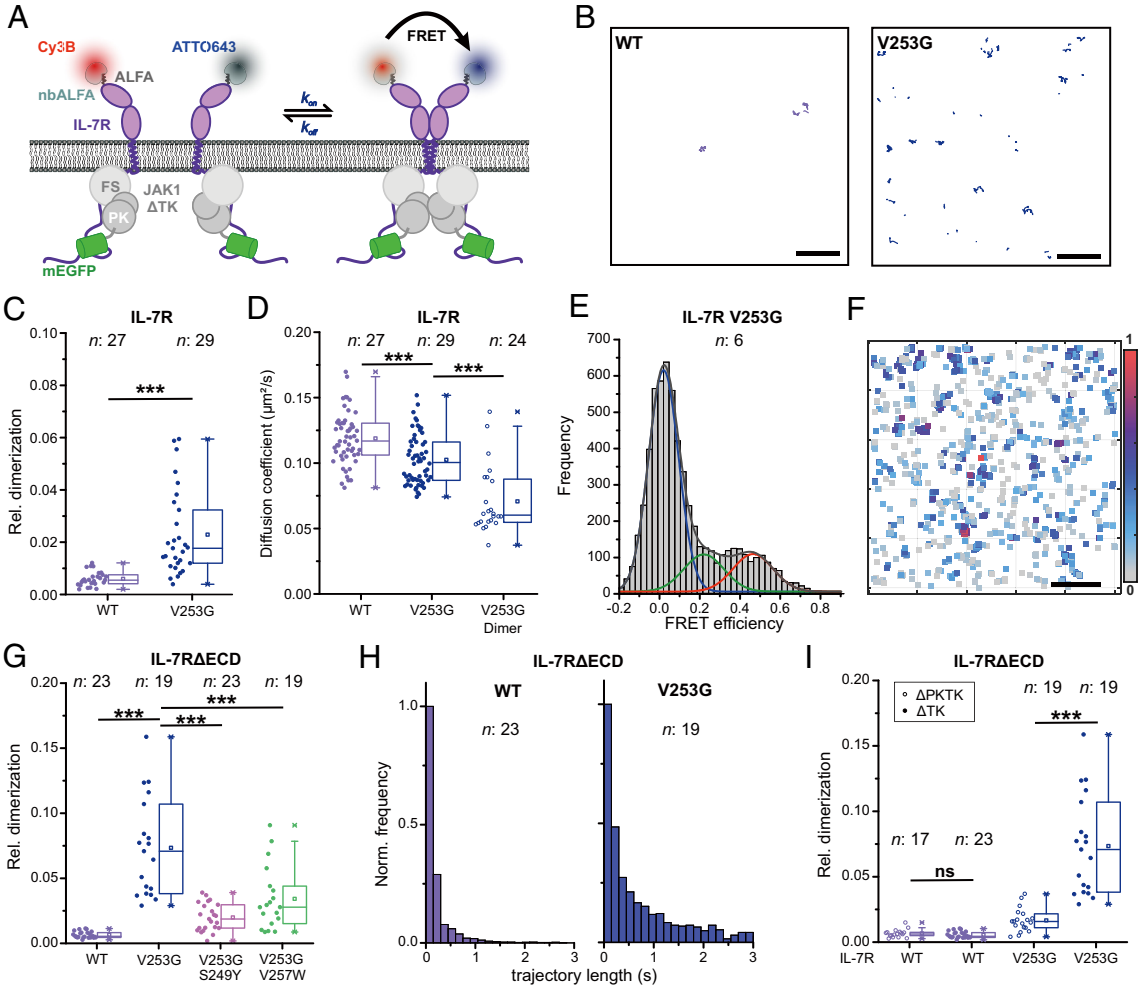


Fig. 4. Ligand-independent dimerization of IL-7R in the plasma membrane of live cells. (*A*) In situ detection of IL-7R V253G dimerization by single-molecule FRET (smFRET) in live cells. IL-7R fused to an N-terminal ALFA-tag was expressed in HeLa cells and labeled in situ with anti-ALFA nanobodies conjugated with donor fluorophore Cy3B or acceptor fluorophore ATTO 643. Dimerization was detected by ALEX-FRET TIRF imaging. (*B*) Representative smFRET trajectories observed for IL-7R WT and V253G, respectively. (Scale bar, 5 μm.) (*C*) Dimerization of IL-7R WT and V253G quantified by smFRET. Data from one representative experiment, with each data point corresponding to the result from one cell. (*D*) Diffusion constants obtained from IL-7R WT and V253G donor and acceptor channel trajectories (solid circle), and V253G-induced cotrajectories (FRET-channel; open circle). Data from one representative experiment, with each data point corresponding to the result from one of *n* cells. (*E*) smFRET efficiency histogram of all colocalized IL-7R V253G pooled from *n* = 6 cells, and fit by multiple Gaussian functions. The peak with a FRET efficiency of ~0 (blue fit curve) corresponds to randomly colocalized donor and acceptor molecules. (*F*) Localization map of colocalized donor and acceptor signals from 150 consecutive frames, color-coded according to the corresponding FRET efficiency. (Scale bar, 5 μm.) (*G*) Comparison of dimerization levels for different IL-7RΔECD variants obtained from cotracking and smFRET detection. Data from three independent experiments, with each data point corresponding to the result from one of *n* cells. (*H*) smFRET trajectory length histograms for IL-7RΔECD WT and V253G dimers from one representative experiment pooled from *n* cells (>1,000 trajectories for each condition). (*I*) Dimerization of IL-7RΔECD V253G in the presence of different JAK1 variants. Data from one representative experiment, with each data point corresponding to the result from one of *n* cells. Statistical significance in *C*, *D*, *G*, and *I* by Student's *t* test. ns, not significant; *$P \le 0.05$; **$P \le 0.01$; ***$P \le 0.001$; ****$P \le 0.0001$.

Downloaded from https://www.pnas.org by CAS SHANGHAI TECH UNIVERSITY on June 11, 2026 from IP address 119.78.253.17.

cells were complemented with JAK1 lacking the tyrosine kinase (TK) domain and fused to a C-terminal mEGFP (JAK1-ΔTK-mEGFP), to ensure receptor integrity while avoiding bias caused by downstream signal activation. HeLa cells transiently expressing ALFA-IL-7R and JAK1-ΔTK-mEGFP were labeled in situ by adding a mixture of ALFAnbs conjugated with donor and acceptor dye, respectively.

Interrogation by total internal reflection fluorescence (TIRF) microscopy with alternating laser excitation (ALEX) revealed individual IL-7R at total densities < 2/μm^2, mostly randomly diffusing in the plasma membrane (*SI Appendix*, Fig. S8*B* and Movie S1). For WT IL-7R, very few, short-lived single-molecule Förster resonance energy transfer (smFRET) events were observed, confirming very low homodimerization propensity (Fig. 4*B* and Movie S1). IL-7R V253G, however, showed a significantly higher level of dimerization, with longer smFRET trajectories (Fig. 4*B* and Movie S1). Quantitative cotracking and smFRET trajectory length analyses confirmed enhanced dimerization levels of V253G compared to WT IL-7R and increased dimer stability (Fig. 4*C* and *SI Appendix*, Fig. S8*C*). Diffusion constants obtained by mean squared displacement (MSD) analysis from single-molecule trajectories confirmed ~40% reduced mobility for V253G-induced IL-7R dimers as compared to the average diffusion of most monomeric IL-7R WT (Fig. 4*D*), in line with previous observations for other class I/II cytokine receptor dimers (20, 33). Quantitative smFRET efficiency analysis for IL-7R V253G dimers yielded a distribution with peaks at 22 and 46% (Fig. 4*E*). This may either indicate a broad distribution of orientations due to high flexibility of the ectodomains or a mixture of two conformers. Localization maps of colocalized IL-7R V253G suggest that the latter may be the case, as trajectories with distinct smFRET efficiencies can be discerned (Fig. 4*F*). However, decisive analysis of potential conformational dynamics is obstructed by the relatively few datapoints within individual trajectories.

For detecting the weak, transient dimerization more robustly, we further increased the FRET efficiency by using IL-7R with its ectodomain replaced by a nonfluorescent monomeric enhanced green fluorescent protein (mXFP-IL-7RΔECD), which was labeled via anti-GFP nanobodies (*SI Appendix*, Fig. S8*D*). Activity assays by phospho-flow cytometry showed similar responsiveness to the V253G mutation for the mXFP-IL-7RΔECD construct as compared to ALFA-IL-7R (*SI Appendix*, Fig. S8*A*). In HeLa cells coexpressing mXFP-tagged IL7RΔECD or IL-7R-V253GΔECD together with JAK1-ΔTK-mEGFP, V253G exhibited substantially higher dimerization than WT (Fig. 4*G* and *SI Appendix*, Fig. S8*E* and Movie S2). The much higher FRET efficiency of ~0.8 enabled tracking of smFRET signals with high fidelity (*SI Appendix*, Fig. S8*F* and Movie S2). Thus, dimer stabilities could be more robustly determined by smFRET trajectory length analysis, confirming substantially increased dimer stability for V253G as compared to WT (*SI Appendix*, Fig. S8 *H* and *I*). Quantitative cotracking and smFRET trajectory length analyses confirmed enhanced dimerization levels and dimer stability for V253G as compared to the WT (Fig. 4 *C* and *D* and *SI Appendix*, Fig. S8*B*). The mutations S249Y and V257W significantly weakened V253G-induced dimerization of IL-7RΔECD and reduced the lifetime of dimers (Fig. 4*G* and *SI Appendix*, Fig. S8 *G–I*), in line with their reduced activity in functional studies (Fig. 3 *F–H*).

To explore potential cooperation between TMD and JAK1 homotypic interactions, we compared dimerization of IL-7RΔECD WT and V253G in the presence of JAK1-ΔTK as well as JAK1 lacking both TK and pseudokinase (PK) domains (JAK1-ΔPKTK). Previous structural and functional studies have shown that productive interaction between the PK domains is relevant for releasing the TK domain and initiating downstream signaling (19, 20, 34). Strikingly, we found significantly reduced dimerization of IL-7RΔECD V253G, but not IL-7RΔECD WT, upon coexpression with JAK1-ΔPKTK (Fig. 4*I*), highlighting that the V253G mutation promotes a TMD dimer geometry compatible with productive interactions between the JAK1 PK domains.

Taken together, our smFRET results demonstrate the new dimerization interface induced by the V253G mutation in live cells and its synergy with JAK1 dimerization between the PK domains, which is a prerequisite for signal activation.

Distinct Activating and Inactivating Homodimerization Interfaces of the IL-7R TMD. The IL-7Rtm-WT at high concentration shows specific intermolecular NOEs on the L255 face of the TMD (Fig. 1), consistent with the MD and biochemical analyses that the WT TMD by itself can homodimerize (Figs. 2 and 3). It is unclear, however, whether this mode of homotypic interaction has any functional consequences. We thus compared the effects of mutating the G253 interface of the V253G mutant and the L255 interface of the WT on ligand-independent receptor signaling. Based on the observation that the V253G mutant but not the WT shows strong signaling in the absence of IL-7 (*SI Appendix*, Fig. S1 *F* and *G*), we hypothesized that TMD homodimerization at the G253 face is structurally compatible with JAK1–JAK1 cross-phosphorylation, whereas TMD homodimerization of the WT at the L255 face is not (Fig. 5*A*). We first examined the effect of single mutations at the L255 face (F251A, L255Y, L255A, I258A, L259A) and found that disrupting the L255 interface indeed reduced dimerization level of IL-7R-TMD (Fig. 5*B*). We then tested the effect of these mutations on STAT5 and JAK1 phosphorylation in BaF3 cells. In the absence of IL-7, single mutations expected to disrupt the packing at the L255 interface – F251A, I258A, and L259A – all exhibited substantially higher levels of p-STAT5 and p-JAK1 than that of the WT (Fig. 5 *C–E*). These unexpected results suggest that TMD dimerization at the L255 face is incompatible with JAK1–JAK1 cross-phosphorylation, as depicted in Fig. 5*A*.

For a direct comparison with the V253G mutant, we also tested single mutations S249Y, S249A, and V257W on top of the V253G mutation that alter the G253 dimerization interface. These mutations all showed dramatic reduction in p-STAT5 and p-JAK1 levels in the absence of IL-7 (Fig. 5 *F–H*). The immunoblotting results overall agree with the smFRET observation that S249Y significantly decreased the mutant dimerization levels on the cell surface (Fig. 4*G*). Addition of IL-7 could increase the level of WT receptor signaling, due to ligand-induced pairing with endogenously expressed γc, but not that of the single mutant V253G and double mutants V253G/S249Y, V253G/S249A, and V253G/V257W (Fig. 5 *I–K*). Thus, these mutations, despite being on the opposite side of the L255 interface recognized by the γc TMD (18), could allosterically weaken IL-7R TMD interaction with the γc TMD.

Collectively, the above results suggest that the dimerization mode of the IL-7R TMD can have profound influence on receptor activation. TMD dimerization at the G253 face can directly activate intracellular JAK1/STAT5 signaling without ligand binding. In contrast, TMD dimerization at the L255 face appears to prevent random JAK1–JAK1 cross-activation and such autoinhibitory mechanism may be important in scenarios of high receptor expression level and high frequency of ligand-independent IL-7R dimerization.

Designed TM Helices Selectively Block Ligand-Independent But Not Ligand-Dependent Signaling. The strong NOEs observed at the homodimer interface of the V253G mutant (Fig. 1*A*)

Downloaded from https://www.pnas.org by CAS SHANGHAI TECH UNIVERSITY on June 11, 2026 from IP address 119.78.253.17.

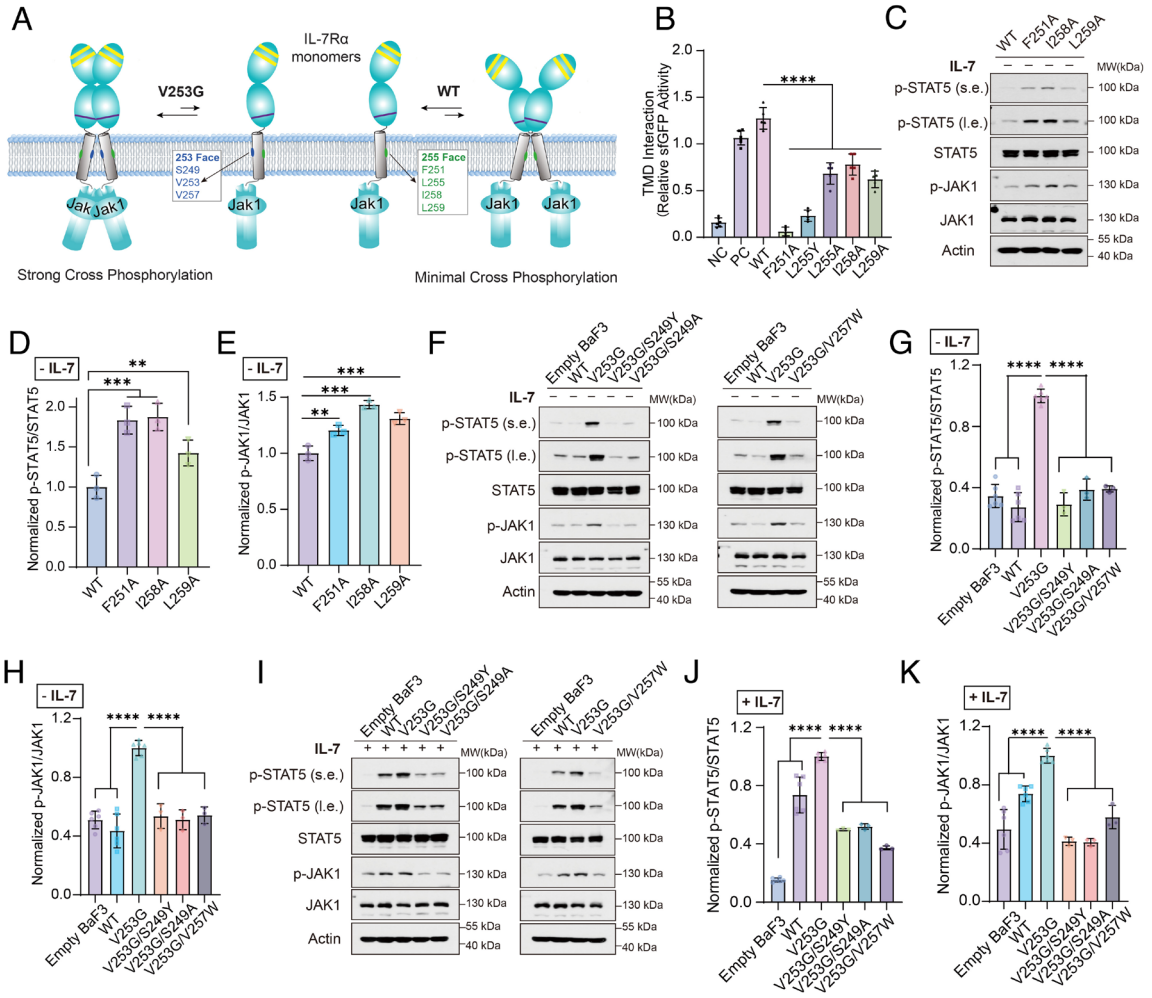


Fig. 5. Activating homodimer of V253G IL-7R vs. inactivating homodimer of WT IL-7R. (*A*) Schematic illustration of activating homodimer of V253G IL-7R and inactivating homodimer of WT IL-7R. In the V253G IL-7R, residues S249, V253, and I257 form the homodimerization interface, which promotes a JAK1–JAK1 pairing configuration that leads to strong cross-phosphorylation. In contrast, the WT IL-7R forms a homodimerization interface composed of F251, L255, I258, and L259, which is incompatible with JAK1–JAK1 cross-phosphorylation. (*B*) TOXGREEN analysis of the impact of single mutations at the L255 face on IL-7R-TMD dimerization. Quantification of sfGFP activity is normalized relative to the GpA positive control. The data are shown as means ± SEMs calculated from technical replicates (typically five to six) from three independent experiments. (*C*) Effect of disrupting the L255 dimerizing face on ligand-independent p-STAT5 and p-JAK1 signals in BaF3 cells. After 5 h of cytokine deprivation, cells expressing WT or mutant IL-7R (F251A, F258A, F259A) were treated with PBS. The p-STAT5 and p-JAK1 signals were detected by immunoblotting and compared with total STAT5 and JAK1, respectively. (*D* and *E*) Quantification of p-STAT5 and p-JAK1 signals in (*C*) as p-STAT5/STAT5 and p-JAK1/JAK1 intensity ratios, normalized to the WT IL-7R. (*F*) Effect of disrupting the G253 dimerizing face on ligand-independent p-STAT5 and p-JAK1 signals in BaF3 cells. After 5 h of cytokine deprivation, cells expressing WT or mutant IL-7R (V253G, V253G/S249Y, V253G/S249A, V257W) were treated with PBS. (*G* and *H*) Quantification of p-STAT5 and p-JAK1 signals in (*F*) as p-STAT5/STAT5 and p-JAK1/JAK1 intensity ratios, normalized to the V253G IL-7R. (*I*) Effect of disrupting the G253 dimerizing face on ligand-dependent p-STAT5 and p-JAK1 signals in BaF3 cells. After 5 h of cytokine deprivation, cells expressing WT or mutant IL-7R (V253G, V253G/S249Y, V253G/S249A, V257W) were treated with 50 ng/mL IL-7. (*J* and *K*) Quantification of p-STAT5 and p-JAK1 signals in (*I*) as p-STAT5/STAT5 and p-JAK1/JAK1 intensity ratios, normalized to the V253G IL-7R. In all quantification graphs, data are shown as means ± SEMs calculated from three independent experiments. Statistical significance by One-way ANOVA. ns, not significant; *$P \le 0.05$; **$P \le 0.01$; ***$P \le 0.001$; ****$P \le 0.0001$. PBS, phosphate-buffered saline. s.e. = short exposure. l.e. = long exposure.

suggest that this non-native, disease-causing interaction is specific. Importantly, the V253G mutation drives homodimerization at G253, whereas the native IL-7R heterodimerizes with γc at residue L255. G253 and L255 lie on opposite faces of the TM helix, indicating that the two dimerizing interactions are noncompetitive, thus offering the opportunity to design a TM peptide (TM_{PEP}) to selectively block the disease-causing homodimerization without affecting the native heterodimerization. We then explored the use of a TM_{PEP} based on the IL-7R TMD sequence, which can compete with TMD homodimerization of the V253G mutant but lacks the receptor ICD necessary for signaling, thus reversing the aberrant signaling caused by the TM mutation. Specifically, the TM_{PEP} contained the V253G mutation for blocking IL-7R mutant homodimerization, or ligand-independent signaling, while simultaneously carrying an L255Y mutation for disrupting the pocket that interacts with the γc TMD, ensuring that it does not interfere with ligand-dependent activation (Fig. 6*A*). A signal sequence was added to the N terminus of the TM_{PEP} to direct it to the plasma membrane upon synthesis. Moreover, a FLAG-tag after the signal sequence was included for probing proper membrane insertion of the TM_{PEP} with anti-FLAG antibody.

To test the above hypothesis, we used two different approaches to deliver designed TM_{PEP} to BaF3 cells: One is lentiviral infection with DNA encoding the TM_{PEP}; in another method, the mRNA coding for the TM_{PEP} was delivered using LNP. For lentiviral infection, the WT TM_{PEP} or mutants (V253G, L255Y, V253G/L255Y, V253/S249Y) were cloned into lentiviral vector with the native IL-7R signal sequence at the N terminus followed by a FLAG-tag, to ensure proper membrane targeting of TM_{PEP} and for detecting protein expression, respectively. Following lentiviral infection of

Downloaded from https://www.pnas.org by CAS SHANGHAI TECH UNIVERSITY on June 11, 2026 from IP address 119.78.253.17.

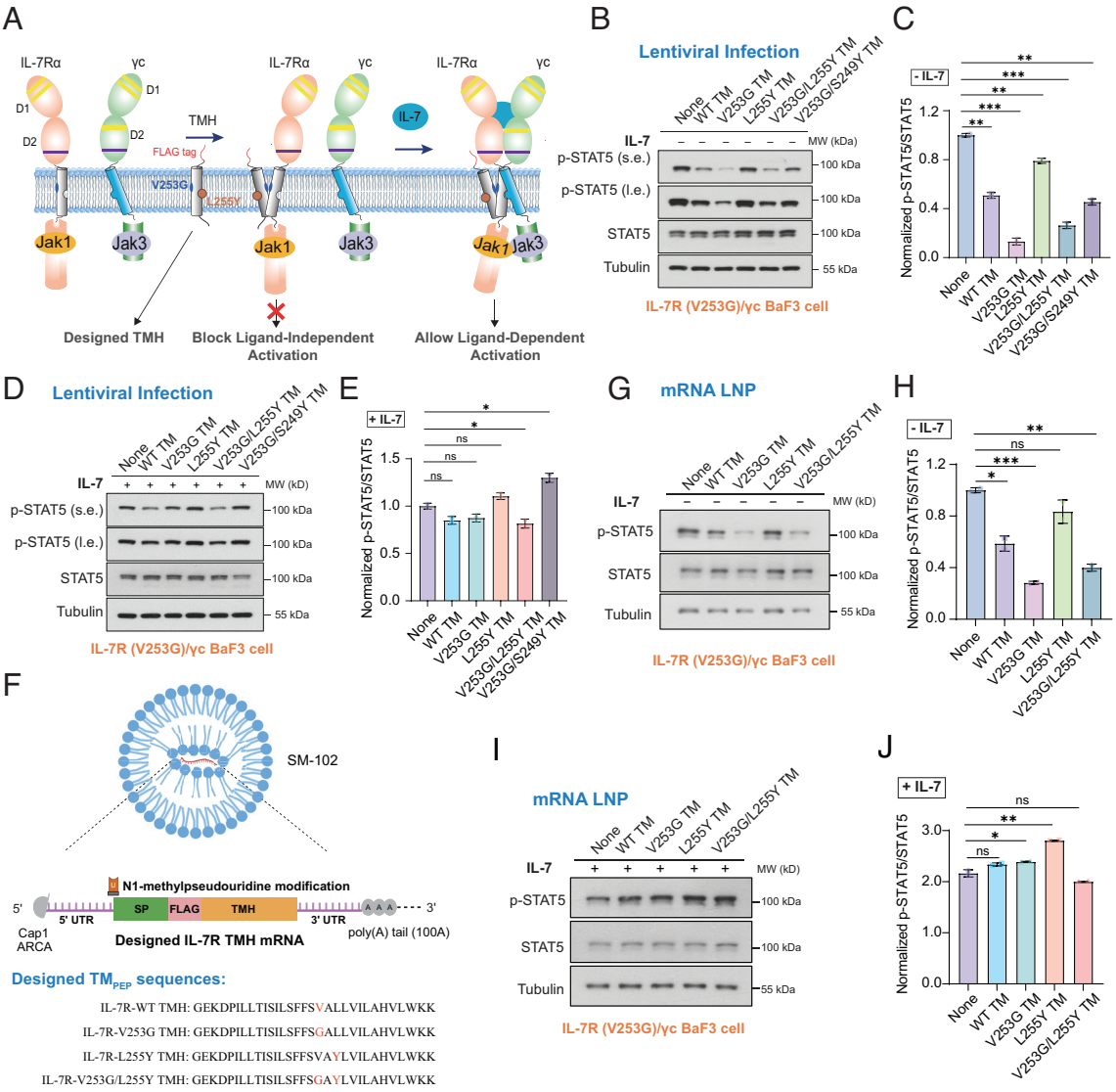


Fig. 6. Selective interference with the oncogenic IL-7R signaling via rational helices design. (*A*) Schematic illustration of the TMD design concept for competitive blocking of IL-7R V253G homodimerization and ligand-independent receptor activation but not affecting IL-7-induced signaling. (*B*) Immunoblot analysis of STAT5 phosphorylation (p-STAT5) in stable BaF3 cells expressing the IL-7R V253G mutant and γc, following lentiviral transduction with WT TM_{PEP} or mutants (V253G, L255Y, V253G/L255Y, V253/S249Y). After 12 h of cytokine deprivation, cells were treated with PBS and collected for immunoblotting. (*C*) Quantification of p-STAT5 signal in (*B*) as p-STAT5/STAT5 intensity ratios, normalized to the no-delivery control (None). (*D*) Immunoblot analysis of p-STAT5 in stable BaF3 cells expressing the IL-7R V253G mutant and γc, following lentiviral transduction with WT TM_{PEP} or mutants as in (*B*). After 12 h of cytokine deprivation, cells were treated with 50 ng/mL IL-7 for 2 h and collected for immunoblotting. (*E*) Quantification of p-STAT5 signal in (*D*) as p-STAT5/STAT5 intensity ratios, normalized to the no-delivery control (None). (*F*) Schematic illustration of the mRNA–LNP delivery system. The mRNA encoding designed TM_{PEP} was delivered into BaF3 cells using lipid nanoparticles (LNPs) comprising ionizable lipids (SM-102) and auxiliary components (*Top*). The mRNAs were modified with N1-methylpseudouridine (m1Ψ) and contained a 5′ Cap1/ARCA and 3′ poly(A) tail (~100A) (*Middle*). The designed TM_{PEP} sequences were listed with mutated residues in red (*Bottom*). (*G*) Immunoblot analysis of p-STAT5 in stable BaF3 cells expressing the IL-7R V253G mutant and γc, following mRNA–LNP delivery of WT TM_{PEP} or mutants (V253G, L255Y, V253G/L255Y, V253/S249Y). After 12 h of cytokine deprivation, cells were treated with PBS and collected for immunoblotting. (*H*) Quantification of p-STAT5 signal in (*G*) as p-STAT5/STAT5 intensity ratios, normalized to the no-delivery control (None). (*I*) Immunoblot analysis of p-STAT5 in stable BaF3 cells expressing the IL-7R V253G mutant and γc, following mRNA–LNP delivery of WT TM_{PEP} or mutants as in (*G*). After 12 h of cytokine deprivation, cells were treated with 50 ng/mL IL-7 for 2 h and collected for immunoblotting. (*J*) Quantification of p-STAT5 signal in (*I*) as p-STAT5/STAT5 intensity ratios, normalized to the no-delivery control (None). Unpaired Student's *t* test was used and data were shown as mean ± SEM calculated from three independent experiments. Represents statistically significant, n.s. (not significant); $*P \le 0.05$, $**P \le 0.01$, $***P \le 0.001$, $****P \le 0.0001$. PBS, phosphate-buffered saline. s.e. = short exposure. l.e. = long exposure.

BaF3 cells expressing the IL-7R V253G mutant and the WT γc, flow cytometry selection using anti-FLAG antibody was performed to generate cell lines stably expressing the TM_{PEP} variants. The cell surface expression levels of the IL-7R V253G mutant and the WT γc were not significantly affected by the transfection of various designed TM_{PEP} (*SI Appendix*, Fig. S9).

In the absence of IL-7 (Fig. 6 *B* and *C*), the V253G mutant again exhibited very robust STAT5 phosphorylation. Upon coexpressing the TM_{PEP} with either single mutation V253G or double mutations V253G/L255Y, which are expected to block homodimerization of the IL-7R V253G mutant, the ligand-independent p-STAT5 signal was drastically reduced by ~70%. Introducing the S249Y on top of the V253G in the TM_{PEP} resulted in weaker inhibition of ligand-independent signaling, consistent with the observation that S249Y can partially disrupt V253G-mediated TMD dimerization. The TM_{PEP} bearing the single mutation L255Y did not show significant inhibition because L255 is not directly involved in dimerization at G253. Interestingly, coexpressing the WT TM_{PEP} also resulted in partial but significant inhibition of tonic signaling (Fig. 6 *B* and *C*), which is likely due

Downloaded from https://www.pnas.org by CAS SHANGHAI TECH UNIVERSITY on June 11, 2026 from IP address 119.78.253.17.

to the minor homodimerization interface on the V253 side of the WT TMD (Fig. 1*B*). In the presence of IL-7, however, coexpression of none of the TM_{PEP} variants showed significant inhibitory effect on STAT5 phosphorylation (Fig. 6 *D* and *E*), likely because the TM_{PEP} cannot compete with the stronger ligand-induced TM heterodimerization of the full-length IL-7R and γc.

In addition to lentiviral infection, we tested the delivery of TM_{PEP} more directly using mRNA encapsulated in LNP, which has been a technology successfully used for vaccine delivery (35). The mRNA encoding WT TM_{PEP} or mutants with N-terminal signal sequence and Flag-tag as above were chemically modified with N1-methylpseudouridine (m1Ψ) and contained a 5′ Cap1/ARCA and 3′ poly(A) tail (~100A) (Fig. 6*F*). These mRNAs were encapsulated in LNPs composed of SM-102, along with auxiliary components essential for nanoparticle stability and efficient delivery. The aforementioned engineered BaF3 stable cells expressing the IL-7R V253G mutant and the γc were starved without cytokines overnight. The starved cells were treated with different mRNA-LNPs and harvested for immunoblotting to examine the effects on downstream JAK/STAT signaling. The results from administration of mRNAs encoding the designed TM_{PEP} are highly consistent with that of the lentiviral infection method, especially in the absence of IL-7 (Fig. 6 *G*–*J*).

Discussion

Naturally occurring GOF mutations within TM regions of single-pass TM receptors have been observed in many types of cytokine and growth factor receptors (1–4, 6, 10). The mechanism of action for these TM mutations has been elusive due to insufficient structural information for the TM and membrane-proximal regions of these receptors as well as the interplay between the TMD and the intracellular signaling domain that allow a TM mutation to activate downstream signaling completely independent of extracellular ligand binding. In this study, we find that the GOF disease mutation V253G residing in the TMD of IL-7R acts by structural rewiring of IL-7R homodimerization leading to intracellular JAK1–JAK1 activation independent of the ligand.

Specifically, the V253G mutation resulted in a major shift of the homotypic TMD dimerization from the L255 interface of the WT (F251, L255, L259) to the G253 interface of the mutant (S249, G253, V257) (Figs. 1 and 2). Interestingly, cysteine substitutions found in the IL-7R TMD from ALL patients are predominantly at residue positions 242 and 249 (9, 11), which are both predicted to crosslink the G253 interface, consistent with the activating TMD dimerization of the V253G mutant. The G253 and L255 homodimerizing interfaces are opposite of each other on the TMD. They also have opposite signaling consequences, as disrupting the G253 interface resulted in drastic reduction of ligand-independent STAT5 and JAK1 phosphorylation, whereas breaking the L255 interface increased ligand-independent signaling (Fig. 5 *C*–*H*). These results suggest that mere TMD dimerization is insufficient for activating intracellular signaling. The TMD needs to dimerize in a specific manner in order to position the JAK1s in an arrangement suitable for initiating cross-phosphorylation. Although the structural link between the TMD and JAK1 is unclear, our smFRET results (Fig. 4*I*) strongly suggest that dimerization through the G253 interface enables productive conformational coupling between the TMD and the PK domain of JAK1 and thus signal activation.

The incompatibility between the L255 interface homodimerization and JAK1 activation could represent a previously unrecognized function of TMD dimerization in receptor control and autoinhibition. Homodimerization of the WT IL-7R TMD via the L255 interface has been observed in the NMR and BACTH analyses, although both showed that it is weaker than the G253 interface dimerization of the mutant TMD (Figs. 1 *A* and *B* and 3 *C* and *D*). The NMR and BACTH experiments, however, were performed at artificially high protein concentration. In the smFRET experiment where the receptor concentration was kept low for single-molecule tracking, the WT showed negligible dimerization which was significantly increased by the V253G mutation (Fig. 4 *B* and *C*). Consistently, MD simulations confirm that the G253 dimer interface is severely destabilized upon reintroducing V253 (Fig. 2*D*). Our previous NMR study also showed that when mixed with the TMD of yc, the L255 interface homodimerization cannot compete with its heterodimerization with the yc TMD (18). The simulations demonstrate that the V253G mutation stabilizes a parallel helix geometry, characterized by similar extracellular (N-terminal) and intracellular (C-terminal) spacings reinforced by W264-mediated aromatic stacking. In contrast, the WT dimer with the L255 interface adopts a crossed-helix arrangement with larger separation at both the extracellular and intracellular sides and lacks W264 stabilization. These structural differences have direct implications for JAK1 positioning and receptor activation, as the reinforced intracellular spacing in the V253G mutant likely enforces an optimal distance and orientation for constitutive JAK1–JAK1 interaction. It is tempting to speculate that the other coreceptor of IL-7R, CRLF2, which also has a Trp residue upstream of the capping Lys (W252), may be recruited via the V253 interface. Interestingly, CRLF2 signals via JAK2, which is more similar to JAK1 than to JAK3; its juxtamembrane segment, which is important for defining functional JAK coupling, is much more similar to IL-7R than to yc. The above clues collectively suggest that the homotypic interaction of the IL-7R TMD at the L255 face is conformationally specific but intrinsically weak. As such, this dimeric interaction may serve as a safety for preventing ligand-independent JAK1 phosphorylation at high receptor concentrations, which can be easily released in the presence of ligand and yc. This safety mechanism, however, cannot prevent dimerization of the G253 interface of the V253G mutant that causes constitutive JAK1 activation. A similar switch of transmembrane dimer interfaces has been proposed to be involved in EGFR activation (28, 36, 37), yet experimental validation in the cellular context has remained controversial (38).

Directly targeting receptor TMD with antibody and small molecule is technically challenging due to additional consideration of lipid binding. Antibodies capable of interacting with the membrane embedded TMDs must also interact with lipids and are thus likely to be polyreactive. Small molecules could in principle either glue or dissociate TMD oligomers to modulate receptor signaling, but the difficulty is also finding the right match between membrane partitioning and TMD interaction. There has been precedence of small molecules targeting receptor TMDs to exert agonistic function. For example, the eltrombopag that activates TpoR by targeting the TMD has been approved for the treatment of idiopathic immune thrombocytopenia (5, 39). In another study of the $p75^{NTR}$, a small molecule was found that can perturb the TMD conformation of the receptor and trigger apoptotic cell death dependent on $p75^{NTR}$ and JNK activity in neurons and melanoma cells (40). Directly targeting receptor TMD has been explored previously with the use of TM peptides. A TM peptide that competes with TM heterodimerization between the integrin α and β subunits could shift the equilibrium from the inactive to active state (41). Furthermore, genetic screen of randomly mutated TMD of the bovine papillomavirus E5 protein identified new TMD sequences that can drive PDGF beta receptor dimerization and activation (42). Similarly, selective inhibition of the

Downloaded from https://www.pnas.org by CAS SHANGHAI TECH UNIVERSITY on June 11, 2026 from IP address 119.78.253.17.

erythropoietin receptor (EpoR) and the T cell receptor by TM peptides has been demonstrated recently (43, 44). These studies suggest that TM helix interactions could afford specificity within the membrane for potentially modulating defective receptor signaling due to TM mutations.

We demonstrate here that, by acquiring solid understanding of the structural basis by which a TMD mutation modulates the activating or inactivating receptor conformation, it is possible to utilize designed TM peptides to specifically suppress the aberrant signaling caused by the TM mutations. In the case of IL-7R, the characterization of a new TMD dimerization mode that supports ligand-independent intracellular JAK1–JAK1 cross-phosphorylation provided a TMD design solution to selectively block ligand-independent but not ligand-dependent IL-7R signaling. With the rapid advancements of gene-based intracellular delivery vehicles for protein drugs such as mRNA and AAV (45, 46), the prospect of clinically addressing disease mutations within the receptor TMDs is no longer just a notional concept.

Materials and Methods

Structural analysis of IL-7Rtm-V253G in membrane-like environment was performed using a previously published Bicelle NMR protocol (22, 23). Molecular modeling of WT IL-7R TMD was performed using Boltz-2 (47). All-atom MD simulations were achieved using tool sets in CHARMM-GUI and GROMACS (48–50). Biochemical analyses of TMD interactions were performed using the BACTH (31) and TOXGREEN (32) assays. Single-molecule imaging of receptor dimerization in live cells was performed using approaches demonstrated previously for cytokine receptors (20). Designed TM helices for mutant signaling interference were introduced into BaF3 cells via lentiviral transduction or mRNA–LNP delivery. Full experimental description is provided in *SI Appendix*.

Data, Materials, and Software Availability. The atomic structure coordinate and structural constraints have been deposited in the Protein Data Bank (PDB) with Accession No. 9XEA (51) (Structure of the transmembrane domain dimer of human IL-7R V253G mutant). ^{1}H, ^{13}C, and ^{15}N chemical shift values have been deposited in the Biological Magnetic Resonance Data Bank (BMRB) with Accession No. 36805 (52). All molecular dynamics simulation files related to this article are publicly available in Zenodo (https://doi.org/10.5281/zenodo.18933507) (53).

ACKNOWLEDGMENTS. We thank A. Zoued and R. Ian for sharing materials for the BACTH assay, the staff at the NMR System/Mass Spectrometry System/Integrated Laser Microscopy System at the National Facility for Protein Science in Shanghai for technical support and assistance in data collection and analysis, and A. Budke-Gieseking, G. Hikade, and W. Kohl for technical support. We thank CSC–IT Center for Science Ltd (Espoo, Finland) for providing computing resources to perform molecular dynamics simulations. We thank Shreyas Kaptan and Felix Eurasto for their help with clustering. This project was supported by the Science and Technology Commission of Shanghai Municipality (22JC1410500), the National Natural Science Fund of China- Research Fund for International Scientists (82350710799) the Strategic Priority Research Program of the Chinese Academy of Sciences (XDB1060000), the Shanghai Basic Research Pioneer Project, the Shanghai Municipal Science and Technology Major Project, and the Chinese Academy of Sciences (2023000040, siocircbc230202) (to J.J.C.); the Deutsche Forschungsgemeinschaft (DFG, German Research Foundation, SFB 1557, 467522186) (to J.P.); National Natural Science Foundation of China (32471354) (to T.C.); the Research Council of Finland grants (331349, 336234, and 346135), the Sigrid Juselius Foundation, Helsinki Institute of Life Science (HiLIFE) Fellow Program, and the Lundbeck Foundation (to I.V.). It was also supported by the China Postdoctoral Science Foundation (2024M763430) and the Shanghai Postdoctoral Excellence Program (2024729) (to Q.W.).

Author affiliations: [a]Interdisciplinary Research Center on Biology and Chemistry, Shanghai Institute of Organic Chemistry, Chinese Academy of Sciences, Shanghai 201210, China; [b]State Key Laboratory of Chemical Biology, Chinese Academy of Sciences, Shanghai 201203, China; [c]Department of Biology/Chemistry and Center for Cellular Nanoanalytics, Osnabrück University, Osnabrück 49076, Germany; [d]Department of Physics, University of Helsinki, Helsinki 00014, Finland; [e]University of Chinese Academy of Sciences, Beijing 101408, China; and [f]Institute of Quantum Sensing, Institute of Fundamental and Transdisciplinary Research, Zhejiang University, Hangzhou, Zhejiang 310027, China

Author contributions: Q.W., M.C., T.C., J.P., and J.J.C. designed research; Q.W., M.C., A.L., S.V., A.Z.C., W.B., Z.D., O.H., G.E., C.P., I.V., and T.C. performed research; Q.W., M.C., A.L., S.V., A.Z.C., W.B., Z.D., O.H., G.E., C.P., I.V., T.C., J.P., and J.J.C. analyzed data; and Q.W., G.E., I.V., J.P., and J.J.C. wrote the paper.

1. C. I. Bargmann, M. C. Hung, R. A. Weinberg, Multiple independent activations of the *neu* oncogene by a point mutation altering the transmembrane domain of p185. *Cell* **45**, 649–657 (1986).
2. S. I. Ou *et al.*, HER2 transmembrane domain (TMD) mutations (V659/G660) that stabilize homo- and heterodimerization are rare oncogenic drivers in lung adenocarcinoma that respond to afatinib. *J. Thorac. Oncol.* **12**, 446–457 (2017).
3. M. Onishi *et al.*, Identification of an oncogenic form of the thrombopoietin receptor MPL using retrovirus-mediated gene transfer. *Blood* **88**, 1399–1406 (1996).
4. J. Ding *et al.*, Familial essential thrombocythemia associated with a dominant-positive activating mutation of the c-MPL gene, which encodes for the receptor for thrombopoietin. *Blood* **103**, 4198–4200 (2004).
5. E. E. Matthews *et al.*, Thrombopoietin receptor activation: Transmembrane helix dimerization, rotation, and allosteric modulation. *FASEB J.* **25**, 2234–2244 (2011).
6. E. Vigano *et al.*, Somatic IL4R mutations in primary mediastinal large B-cell lymphoma lead to constitutive JAK-STAT signaling activation. *Blood* **131**, 2036–2046 (2018).
7. L. W. Campos, L. G. Pissinato, J. A. Yunes, Deleterious and oncogenic mutations in the IL7RA. *Cancers (Basel)* **11**, 1952 (2019).
8. A. M. Savino, S. Izraeli, Interleukin-7 signaling as a therapeutic target in acute lymphoblastic leukemia. *Expert Rev. Hematol.* **10**, 183–185 (2017).
9. C. Shochat *et al.*, Gain-of-function mutations in interleukin-7 receptor-alpha (IL7R) in childhood acute lymphoblastic leukemias. *J. Exp. Med.* **208**, 901–908 (2011).
10. C. Shochat *et al.*, Novel activating mutations lacking cysteine in type I cytokine receptors in acute lymphoblastic leukemia. *Blood* **124**, 106–110 (2014).
11. P. P. Zenatti *et al.*, Oncogenic IL7R gain-of-function mutations in childhood T-cell acute lymphoblastic leukemia. *Nat. Genet.* **43**, 932–939 (2011).
12. T. J. Fry, C. L. Mackall, Interleukin-7: From bench to clinic. *Blood* **99**, 3892–3904 (2002).
13. R. Mazzucchelli, S. K. Durum, Interleukin-7 receptor expression: Intelligent design. *Nat. Rev. Immunol.* **7**, 144–154 (2007).
14. Y. Rochman, R. Spolski, W. J. Leonard, New insights into the regulation of T cells by gamma(c) family cytokines. *Nat. Rev. Immunol.* **9**, 480–490 (2009).
15. W. J. Leonard, Cytokines and immunodeficiency diseases. *Nat. Rev. Immunol.* **1**, 200–208 (2001).
16. S. T. Walsh, Structural insights into the common gamma-chain family of cytokines and receptors from the interleukin-7 pathway. *Immunol. Rev.* **250**, 303–316 (2012).
17. X. Wang, P. Lupardus, S. L. Laporte, K. C. Garcia, Structural biology of shared cytokine receptors. *Annu. Rev. Immunol.* **27**, 29–60 (2009).
18. T. Cai, R. Lenoir Capello, X. Pi, H. Wu, J. J. Chou, Structural basis of γ chain family receptor sharing at the membrane level. *Science* **381**, 569–576 (2023).
19. N. A. Caveney *et al.*, Structural basis of Janus kinase trans-activation. *Cell Rep.* **42**, 112201 (2023).
20. S. Wilmes *et al.*, Mechanism of homodimeric cytokine receptor activation and dysregulation by oncogenic mutations. *Science* **367**, 643–652 (2020).
21. M. E. Call, J. J. Chou, A view into the blind spot: Solution NMR provides new insights into signal transduction across the lipid bilayer. *Structure* **18**, 1559–1569 (2010).
22. Q. Fu, A. Piai, W. Chen, K. Xia, J. J. Chou, Structure determination protocol for transmembrane domain oligomers. *Nat. Protoc.* **14**, 2483–2520 (2019).
23. A. Piai, Q. Fu, J. Dev, J. J. Chou, Optimal bicelle size q for solution NMR studies of the protein transmembrane partition. *Chemistry* **23**, 1361–1367 (2017).
24. C. R. Sanders 2nd, J. P. Schwonek, Characterization of magnetically orientable bilayers in mixtures of dihexanoylphosphatidylcholine and dimyristoylphosphatidylcholine by solid-state NMR. *Biochemistry* **31**, 8898–8905 (1992).
25. D. Schneider, D. M. Engelman, Motifs of two small residues can assist but are not sufficient to mediate transmembrane helix interactions. *J. Mol. Biol.* **343**, 799–804 (2004).
26. M. G. Teese, D. Langosch, Role of GxxxG motifs in transmembrane domain interactions. *Biochemistry* **54**, 5125–5135 (2015).
27. K. R. MacKenzie, J. H. Prestegard, D. M. Engelman, A transmembrane helix dimer: Structure and implications. *Science* **276**, 131–133 (1997).
28. N. F. Endres *et al.*, Conformational coupling across the plasma membrane in activation of the EGF receptor. *Cell* **152**, 543–556 (2013).
29. K. S. Mineev *et al.*, Spatial structure of the transmembrane domain heterodimer of ErbB1 and ErbB2 receptor tyrosine kinases. *J. Mol. Biol.* **400**, 231–243 (2010).
30. L. Pan *et al.*, Higher-order clustering of the transmembrane anchor of DR5 drives signaling. *Cell* **176**, 1477–1489.e1414 (2019).
31. A. Battesti, E. Bouveret, The bacterial two-hybrid system based on adenylate cyclase reconstitution in *Escherichia coli*. *Methods* **58**, 325–334 (2012).
32. C. R. Armstrong, A. Senes, Screening for transmembrane association in divisome proteins using TOXGREEN, a high-throughput variant of the TOXCAT assay. *Biochim. Biophys. Acta* **1858**, 2573–2583 (2016).
33. J. Sotolongo Bellón *et al.*, Four-color single-molecule imaging with engineered tags resolves the molecular architecture of signaling complexes in the plasma membrane. *Cell Rep. Methods* **2**, 100165 (2022).
34. C. R. Glassman *et al.*, Structure of a Janus kinase cytokine receptor complex reveals the basis for dimeric activation. *Science* **376**, 163–169 (2022).
35. M. G. Alameh *et al.*, Lipid nanoparticles enhance the efficacy of mRNA and protein subunit vaccines by inducing robust T follicular helper cell and humoral responses. *Immunity* **55**, 1136–1138 (2022).

Downloaded from https://www.pnas.org by CAS SHANGHAI TECH UNIVERSITY on June 11, 2026 from IP address 119.78.253.17.

36. S. J. Fleishman, J. Schlessinger, N. Ben-Tal, A putative molecular-activation switch in the transmembrane domain of ErbB2. *Proc. Natl. Acad. Sci. U.S.A.* **99**, 15937–15940 (2002).
37. E. V. Bocharov *et al.*, Alternative packing of EGFR transmembrane domain suggests that protein–lipid interactions underlie signal conduction across membrane. *Biochim. Biophys. Acta* **1858**, 1254–1261 (2016).
38. L. C. Zanetti-Domingues *et al.*, The architecture of EGFR's basal complexes reveals autoinhibition mechanisms in dimers and oligomers. *Nat. Commun.* **9**, 4325 (2018).
39. D. J. Kuter, Thrombopoietin and thrombopoietin mimetics in the treatment of thrombocytopenia. *Annu. Rev. Med.* **60**, 193–206 (2009).
40. E. T. H. Goh *et al.*, A small molecule targeting the transmembrane domain of death receptor p75(NTR) induces melanoma cell death and reduces tumor growth. *Cell Chem. Biol.* **25**, 1485–1494.e1485 (2018).
41. H. Yin *et al.*, Computational design of peptides that target transmembrane helices. *Science* **315**, 1817–1822 (2007).
42. L. L. Freeman-Cook *et al.*, Selection and characterization of small random transmembrane proteins that bind and activate the platelet-derived growth factor beta receptor. *J. Mol. Biol.* **338**, 907–920 (2004).
43. M. Mravic *et al.*, De novo-designed transmembrane proteins bind and regulate a cytokine receptor. *Nat. Chem. Biol.* **20**, 751–760 (2024).
44. Y. Ye *et al.*, Allosteric inhibition of the T cell receptor by a designed membrane ligand. *eLife* **12**, e82861 (2023).
45. P. S. Kowalski, A. Rudra, L. Miao, D. G. Anderson, Delivering the messenger: Advances in technologies for therapeutic mRNA delivery. *Mol. Ther.* **27**, 710–728 (2019).
46. D. Wang, P. W. L. Tai, G. Gao, Adeno-associated virus vector as a platform for gene therapy delivery. *Nat. Rev. Drug Discov.* **18**, 358–378 (2019).
47. S. Passaro *et al.*, Boltz-2: Towards accurate and efficient binding affinity prediction. bioRxiv [Preprint] (2025). https://doi.org/10.1101/2025.06.14.659707 (Accessed 10 April 2026).
48. S. Feng, S. Park, Y. K. Choi, W. Im, CHARMM-GUI membrane builder: Past, current, and future developments and applications. *J. Chem. Theory Comput.* **19**, 2161–2185 (2023).
49. J. Huang *et al.*, CHARMM36m: An improved force field for folded and intrinsically disordered proteins. *Nat. Methods* **14**, 71–73 (2017).
50. M. J. Abraham *et al.*, GROMACS: High performance molecular simulations through multi-level parallelism from laptops to supercomputers. *SoftwareX* **1–2**, 19–25 (2015).
51. Q. Wang, T. Cai, J. J.Chou, Structure of the transmembrane domain dimer of human IL-7R V253G mutant. Protein Data Bank. https://www.rcsb.org/structure/9XEA. Deposited 27 October 2025.
52. Q. Wang, T. Cai, J. J. Chou, Structure of the transmembrane domain dimer of human IL-7R V253G mutant. Biological Magnetic Resonance Data Bank. https://bmrb.io/data_library/summary/index.php?bmrbId=36805. Deposited 27 October 2025.
53. Q. Wang *et al.*, Structural rewiring of IL-7R dimerization by an oncogenic transmembrane mutation can be reversed by rational design [Data set]. Zenodo. https://doi.org/10.5281/zenodo.18933507. Accessed 10 April 2026.

Downloaded from https://www.pnas.org by CAS SHANGHAI TECH UNIVERSITY on June 11, 2026 from IP address 119.78.253.17.